A Sulfur-Rich Copolymer@CNT Hybrid Cathode with Dual-Confinement of Polysulfides for High-Performance Lithium–Sulfur Batteries

Guangjian Hu, Zhenhua Sun, Chao Shi, Ruopian Fang, Jing Chen, Pengxiang Hou, Chang Liu, Hui-Ming Cheng, and Feng Li**

Lithium–sulfur (Li—S) batteries based on a multielectron chemical reaction have been investigated as a promising electrochemical energy storage system owing to their high theoretical energy density, low cost, and environmental friendliness.[1,2] However, Li—S batteries still suffer from some essential problems that hinder their use. First, both sulfur and the final discharge product (Li_2S) have very poor ionic and electronic conductivities.[3] Second, the dissolution of polysulfide ions in an organic electrolyte leads to a reaction with the lithium anode and causes the so-called "shuttle effect".[4] Third, the large volumetric expansion of sulfur upon lithiation results in electrode damage and cell degradation.[5] As a result, Li—S batteries show poor cycling stability and low Coulombic efficiency.[6]

Extensive efforts have been devoted to solving these problems by structure design through physical or chemical confinement. In a pioneering study by Nazar and co-workers mesoporous carbon was used to encapsulate or trap S/Li_2S active material as well as polysulfides within the conductive host material.[1] A similar physical-confinement method was subsequently reported for the preparation of sulfur hybrids with macro-/meso-/microporous carbons[7] and carbon nanotubes (CNTs)/nanofibers.[8] Although these carbon–sulfur hybrids have shown better electrochemical performance during initial charge/discharge cycles, their performance usually decreases rapidly in subsequent cycles because the physical confinement alone is insufficient and kinetically unfavorable for tackling the polysulfide-shuttle issue.

In this respect, researchers have developed chemical-confinement methods by directly using elemental sulfur as a feedstock to form chemically stable copolymers.[9] Due to the strong chemical interaction of sulfur with the carbon framework in C—S copolymers, the dissolution of polysulfides and their diffusion out of the cathode is effectively suppressed by chemical binding. Recently, Pyun and co-workers proposed a novel sulfur-rich polymer with 90 wt% sulfur content formed by an organic free radical reaction.[10] The initial discharge capacity of the Li–S batteries fabricated using this copolymer as cathode reached 1100 m Ah g^{-1} at 0.1 C, but rapidly decreased to less than 400 m Ah g^{-1} at 2 C. Inspired by this idea, Meng and co-workers used a sulfur-rich polymeric material produced by the copolymerization of elemental sulfur with 1,3-diethynylbenzene,[11] which exhibited an initial specific capacity of 1143 m Ah g^{-1} at 0.1 C, and 595 m Ah g^{-1} at 1 C. Although these sulfur copolymers open a new approach for the use of chemically confined polysulfides in Li–S batteries, their poor conductivity has prevented the achievement of good cycling and rate performance.

Based on the above studies, a well-designed structure of a carbon–sulfur matrix cathode using physical and/or chemical confinement is crucially important for high performance Li–S batteries. To summarize, a sulfur-based cathode should not only be highly conductive to improve the utilization of sulfur, but also capable of effectively confining polysulfide ions to prevent their dissolution and accommodate the significant volume changes caused by lithium insertion/extraction. Here, we report a sulfur-rich polymer@CNT hybrid cathode for Li–S batteries produced by combining the physical and chemical confinement strategies. This well-designed structure has several advantages: (1) the nanoscale sulfur copolymer enables high active material utilization; (2) the CNTs hollow core serves as a nanoscale electrochemical reaction vessel that efficiently confines active materials; (3) the unfilled space of CNTs can accommodate sulfur volume expansion; (4) the conductive CNTs provides paths for fast electron transport; (5) the π electrons of the aromatic sulfur copolymer rings enhance Li^+ transfer; (6) the strong chemical interaction of sulfur with the carbon framework (C—S bonds) inhibits the "shuttle effect." The combination of the physical confinement of lithium polysulfide ions in hollow CNTs and the strong chemical binding of C to S in the copolymer compounds suppresses sulfur loss during discharge/charge processes. A sulfur-1,3-diisopropenylbenzene@CNT (S-DIB@CNT) membrane cathode gives a high specific capacity of 1300 m Ah g^{-1} at 0.1 C, a high-rate capacity of 700 m Ah g^{-1} at 2 C and excellent cycling stability for 100 cycles with a high specific capacity of 880 m Ah g^{-1} at 1 C.

Figure 1a shows the preparation process of the S-DIB copolymer by inverse vulcanization through direct dissolution and copolymerization of DIB in liquid sulfur.[10] This process was conducted at 185 °C to promote efficient free radical ring-opening polymerization of S_8 and resulted in a chemically stable S-DIB copolymer with a red color (Figure S1, Supporting

G. J. Hu, Dr. Z. H. Sun, C. Shi, R. P. Fang, J. Chen, Prof. P. X. Hou, Prof. C. Liu, Prof. H.-M. Cheng, Prof. F. Li
Shenyang National Laboratory for Materials Science
Institute of Metal Research
Chinese Academy of Sciences
Shenyang 110016, China
E-mail: cliu@imr.ac.cn; fli@imr.ac.cn
Prof. H.-M. Cheng
Tsinghua-Berkeley Shenzhen Institute
Tsinghua University
Shenzhen 518055, China

DOI: 10.1002/adma.201603835

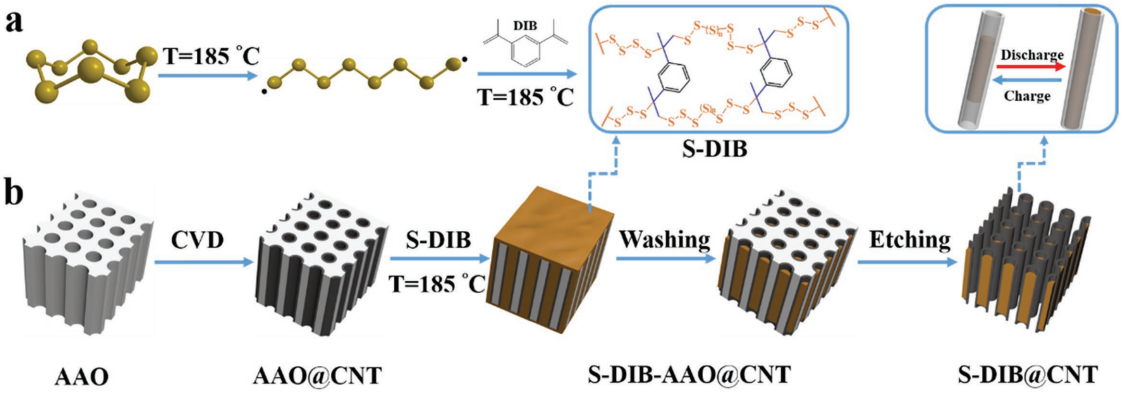

Figure 1. a) Synthesis scheme of the S-DIB copolymer. b) Schematic showing the fabrication process of the S-DIB@CNT hybrid.

Information). The synthesis of the S-DIB@CNT hybrid is illustrated in Figure 1b. First, CNTs were prepared by the chemical vapor deposition of acetylene on the channel surface of an anodic aluminum oxide (AAO) template (Figures S2 and S3, Supporting Information). The as-prepared copolymer (S-DIB) was infiltrated into the AAO@CNT host by melt diffusion and excess S-DIB covering the AAO surface was removed by washing with carbon disulfide (CS_2). Second, the sample was immersed in a 5M NaOH solution to remove the AAO template followed by repeated rinsing with purified water. Finally, the wet S-DIB@CNT hybrid was subjected to vacuum filtration to produce a membrane cathode.

The morphologies of the as-synthesized S-DIB@CNT hybrid were characterized using scanning electron microscopy (SEM). From a low magnification SEM image (**Figure 2**a), many CNT bundles can be observed. The S-DIB content can be controlled by rinsing with CS_2 solution so that there is sufficient free space for sulfur to expand during the formation of Li_2S (Figure 2b). After filling the CNT cores with S-DIB the initial morphology of the CNT is retained without excess S-DIB observed on the CNT walls (Figure 2c). S-DIB@CNT hybrid membranes about 4 cm in diameter were prepared by vacuum filtration and were used as a binder-free cathode without a metal current collector (Figure 2d).[12] Carbon and sulfur in the S-DIB@CNT hybrid membrane were also confirmed by elemental maps (Figure S4, Supporting Information).

To further confirm the distribution of the sulfur-rich copolymer in the CNTs, we used transmission electron microscopy (TEM). **Figure 3**a and Figure S5a,b (Supporting Information) show TEM images of a CNT partially filled with S-DIB. The CNTs have a wall thickness of ≈10 nm and a hollow core diameter of ≈200 nm. High-resolution TEM (HRTEM) images show that the CNT wall is not well crystallized due to the relatively low synthesis temperature (Figure 3b), and this feature is important for allowing fast lithium ion diffusion. Further evidence showing the filling of the core of the CNTs with the sulfur copolymer was provided by scanning transmission electron microscopy (STEM) (Figure 3c and Figure S5c,d, Supporting Information). From TEM and STEM images, we can see that each hollow CNT serves as a nanoscale electrochemical reactor, providing physical entrapment of polysulfide ions and internal void space to accommodate the volume expansion of sulfur during lithiation. The elemental maps show the spatial

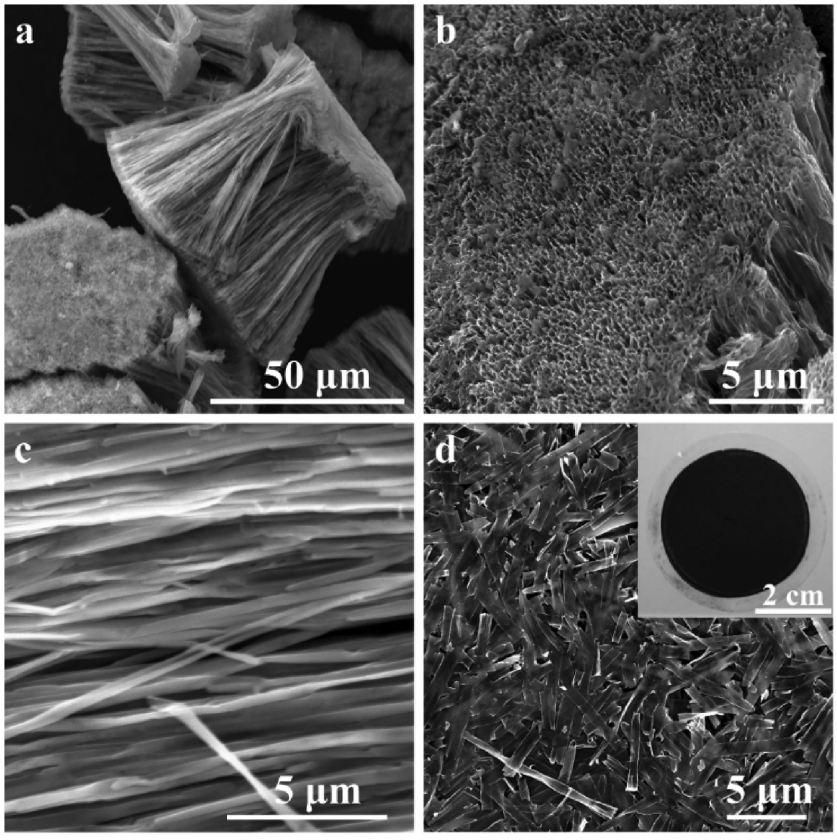

Figure 2. SEM images of the as-prepared S-DIB@CNT hybrid. a) Low magnification, b) top view, and c) cross-sectional view. d) Interwoven S-DIB@CNT hybrid network in a membrane and an optical photograph of the membrane (inset).

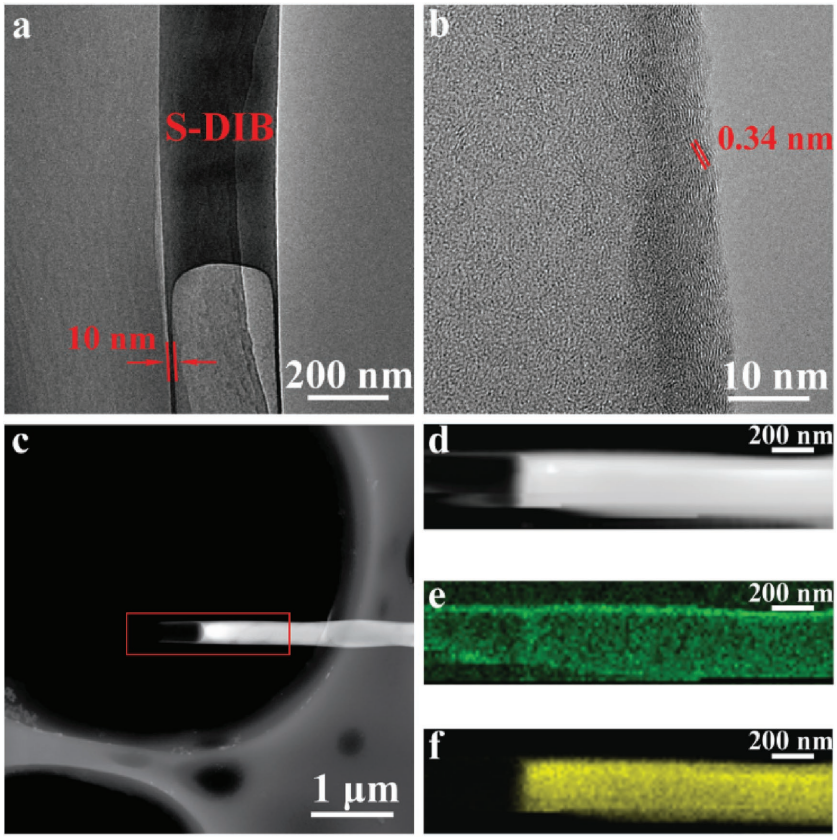

Figure 3. a) TEM characterization of an isolated partially S-DIB-filled CNT. b) HRTEM image of the CNT wall. c,d) HAADF-STEM images of the S-DIB@CNT hybrid. e,f) EDX elemental maps of carbon (green) and sulfur (yellow) in the area marked with a rectangle in (c).

distributions of sulfur and carbon (Figure 3d–f), indicating that the S-DIB is homogeneously encapsulated only in the hollow cores of the CNTs.

For comparison, a S@CNT hybrid membrane was prepared by the method described above (Figure S6, Supporting Information). The contents of active material in the S@CNT and S-DIB@CNT were determined by thermogravimetry analysis (TGA) to be 67 and 63.5 wt%, respectively (**Figure 4**a and Figure S7a, Supporting Information). Comparison of the active material content of S-DIB@CNT (63.5 wt%) with the highest active content of previously reported CNT-encapsulated composites (92.1 wt%),[13] showed that the extra space for sulfur volume expansion generated by the CS_2 washing could reach ≈30%. This void space can accommodate ≈50% volume expansion of the sulfur present in the hollow CNTs.[5] To further understand the physical and chemical interaction of sulfur with DIB in the CNTs, Raman spectroscopy, X-ray diffraction (XRD), X-ray photoelectron spectroscopy (XPS), and nuclear magnetic resonance (NMR) spectra were used. As can be seen in Figure 4b and Figure S7b (Supporting Information), the Raman spectrum of the CNTs shows the typical pattern of a partially graphitized carbon with two main peaks of the D band and G band (I_D: I_G = 1.02). Due to the high sulfur content (90 wt%) in the S-DIB copolymer, the S-DIB shows a Raman pattern consistent with sulfur powder. However, the characteristic peaks of S and S-DIB cannot be observed for the S@CNT and S-DIB@CNT hybrids, indicating that the sulfur is completely inside the CNTs.[12,14] XRD was also performed to understand the crystal phase changes of the S@CNT and S-DIB@CNT hybrids (Figure 4c and Figure S7c, Supporting Information). The XRD pattern of the S-DIB confirmed the presence of long-chain elemental sulfur with the orthorhombic structure of elemental sulfur. In contrast, the intensity of sulfur peaks was much weaker in the S@CNT and S-DIB@CNT hybrids,[13,15] which agrees with the Raman analysis indicating the excellent physical confinement of sulfur inside the CNTs.[13,16] The S element was also confirmed by S 2p peaks in XPS spectra (Figure S8, Supporting Information). Compared with the XPS spectra of S@CNT, the noticeable C—S peak (≈162.1 eV) of S-DIB@CNT indicated the existence of bonding interactions between the C atom and S atom in S-DIB copolymer.[17] Solution ^{1}H and ^{13}C NMR spectroscopy were used to confirm the formation of C—S bonds from S-DIB copolymerization.[10] A survey of the ^{1}H NMR spectrum of the S-DIB copolymer confirms the presence of aromatic peaks at δ = 6.8–7.8 ppm and methyl protons at δ = 1.0–2.2 ppm (Figure 4d). Resonances at δ = 2.9–3.4 ppm correspond to methylene peaks in the DIB backbone, which are bonded to sulfur comonomer units. ^{13}C NMR analysis further confirmed the formation of copolymers and the presence of C—S bonds (Figure S7d, Supporting Information). The presence of methylene carbons from DIB directly bonded to sulfur units was observed at δ = 48 ppm and quaternary carbons of DIB bonded to sulfur units were also observed at δ = 55 ppm.[10]

The electrochemical performance of the S@CNT and S-DIB@CNT hybrids as membrane cathodes was investigated (**Figure 5**) and cyclic voltammetry (CV) data obtained at a scan rate of 0.05 mV s^{-1} in the voltage range of 1.7–2.8 V versus Li/Li^+ are presented in Figure 5a. The two main reduction peaks for both the S_8 and S-DIB copolymer are similar. The 2.28–2.32 V and 1.98–2.01 V at high potentials can be attributed to the reduction of sulfur to long-chain lithium polysulfide ions and the S-DIB copolymer to higher order organosulfur DIB units; and organosulfur DIB units with shortened oligosulfur units were generated upon further reactions. Continued discharge into the lower voltage plateau resulted in Li_2S_2/Li_2S and the conversion of oligosulfur units into fully discharged organosulfur DIB products. In the subsequent anodic scan, two broad oxidation peaks at 2.35–2.47 V for both S@CNT and S-DIB@CNT are attributed to the conversion of short-chain polysulfide ions to long-chain, and these have been observed in a few sulfur-conductive matrix materials,[12,18] indicating significantly improved reversibility, high conductivity, and low polarization. These analyses therefore confirm that the S-DIB copolymer has similar electrochemical behavior to

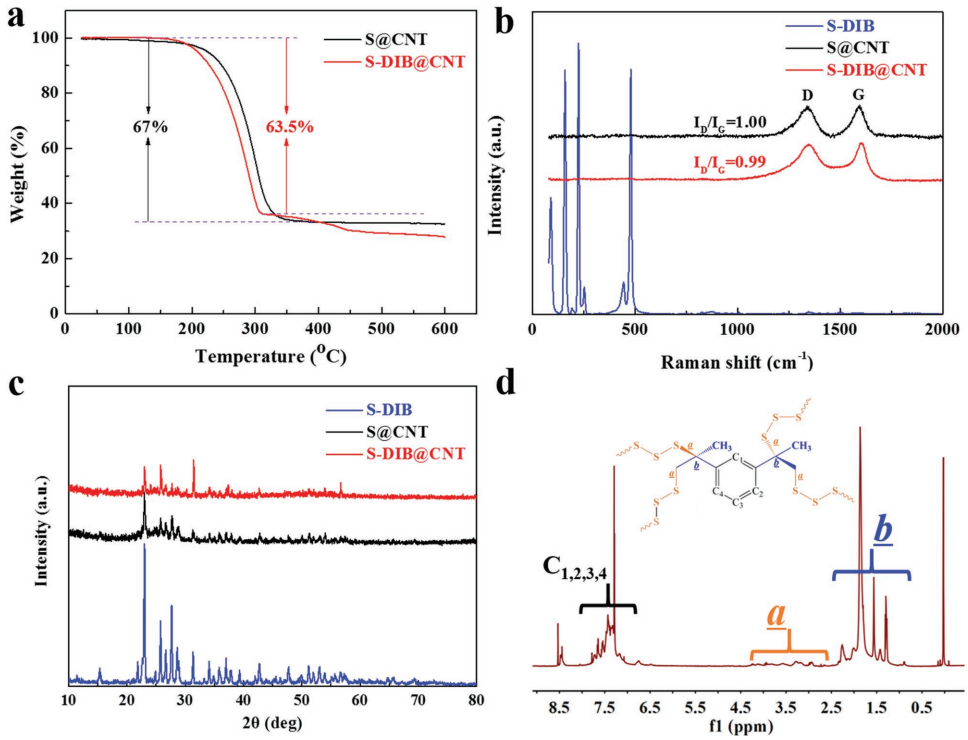

Figure 4. a) TGA curves of the S@CNT and S-DIB@CNT hybrid. b) Raman spectra of the S-DIB, S@CNT, and S-DIB@CNT materials. c) XRD patterns of the S-DIB copolymer, S@CNT, and S-DIB@CNT materials. d) ^{1}H-NMR spectrum of the S-DIB copolymer.

S_8.[10] Moreover, the subsequent cyclic voltammetric curves of S-DIB cathode are in agreement with the reversible reaction (Figure S9, Supporting Information).

Figure 5b shows typical charge–discharge curves of the S@CNT and S-DIB@CNT hybrids at 0.1 and 1 C rates. They consist of two well-defined charge and discharge plateaus, in

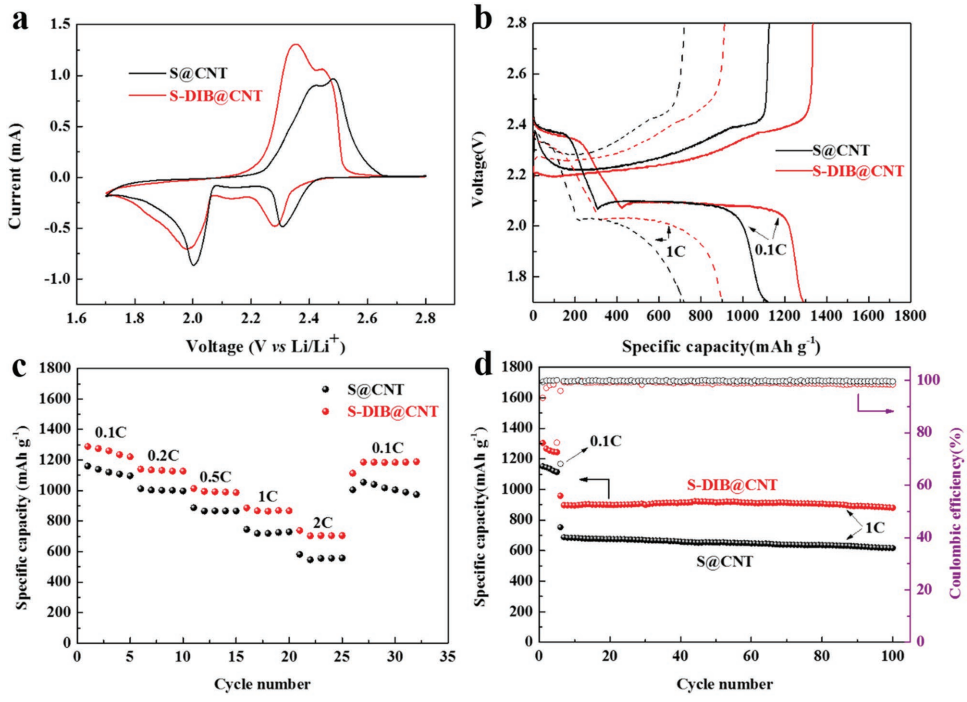

Figure 5. a) CV curves, b) charge–discharge profiles at different rates (solid line 0.1 C, dashed line 1 C), c) rate performance at stepwise current rates, and d) cycling performance at 1 C of the S@CNT and S-DIB@CNT hybrids.

agreement with the CV curves in subsequent cycles. Compared with the CV curves of the S@CNT, a high-potential plateau appears at about 2.35 V for the S-DIB@CNT, exhibiting a capacity of 418 m Ah g^{-1}. The discharge profile matches the theoretical prediction very well,[19] leading us to conclude that linear polysulfane in the S-DIB copolymer with no ring-opening facilitates fast reaction kinetics. It should also be noted that, after the first cycle, the CV curves of S-DIB@CNT showed an obvious positive shift in the reduction peak and a negative shift in the oxidation peak, indicating a decrease in cell polarization.[18] The Nyquist plots of the S@CNT and S-DIB@CNT cathodes are similar with a typical semicircle in the high-medium frequency region and an inclined line at the low frequency region, which can be ascribed to the charge-transfer resistance and a mass-transfer process (Figure S10, Supporting Information).[20] R_{ct} value of the S-DIB@CNT cathode (95 Ω) is lower than that of the S@CNT (115 Ω), implying that the π electrons of the S-DIB copolymer increase the Li^+ transfer rate that has smaller electrochemical reaction resistance to facilitate charge-transfer in the whole battery system.[17,21] This result suggests that the π electrons of the S-DIB copolymer can increase the Li^+ transfer rate.[17] Because of the fast Li^+ transport in the S-DIB@CNT, the galvanostatic charge–discharge behavior was evaluated at different rates. As shown in Figure 5c, the S-DIB@CNT membrane cathode delivered a capacity of 1300 m Ah g^{-1} at 0.1 C, 1130 m Ah g^{-1} at 0.2 C, 990 m Ah g^{-1} at 0.5 C, 890 m Ah g^{-1} at 1 C, and 700 m Ah g^{-1} at 2 C. When the current density returned to 0.1 C, these cells resumed a capacity of over 1180 m Ah g^{-1}, showing good capacity retention. In comparison the previous reports of work in which S-DIB was directly used as the electrode,[10] our S-DIB@CNT material showed a much higher rate capability due to the combination of physical and chemical-confinement. The performance of the S@CNT cathode was also measured. Like most S@CNT cathodes, it showed rapidly decreased capacities of 720 m Ah g^{-1} at 1 C and 550 m Ah g^{-1} at 2 C, indicating insufficient physical confinement when using pure sulfur.

In order to further explore the advantage of this dual confinement strategy, the cycling performance of the S-DIB@CNT and S@CNT cathodes was evaluated. As demonstrated in Figure 5d, after being activated at 0.1 C in the initial five cycles, the S-DIB@CNT delivered a discharge capacity of 898 m Ah g^{-1}, and is able to maintain a stable reversible discharge capacity of 880 m Ah g^{-1} (capacity retention of 98%) with a high Coulombic efficiency of 99% for 100 cycles at 1 C. In contrast, although the S@CNT electrode delivered a discharge capacity of 687 m Ah g^{-1} in the first cycle, it only retained a discharge capacity of 617 m Ah g^{-1} (capacity retention of 89.8%) after 100 cycles. The average capacity fade rate for the S-DIB@CNT was calculated to be ≈0.02% per cycle, much smaller than ≈0.1% for the S@CNT. Under the same experimental conditions, it was confirmed that the presence of the C—S bond in the S-DIB copolymer has taken the chemical-confinement function of polysulfides during the charge–discharge process of Li—S batteries.[22] Figure S11 (Supporting Information) shows the surface morphology and EDS elemental mappings of the S-DIB@CNT hybrid membrane after 100 cycles. There is no obvious volume change for the CNTs due to their robustness and void space for accommodating the sulfur volume expansion, which leads to good structural stability of the cathode during cycling. Moreover, there is no bulk S-DIB observed on the surface of the membrane cathode, indicating the efficient confinement of S-DIB in CNTs. EDS elemental mapping shows a uniform distribution of sulfur in the CNTs, which suggests that the CNT membrane acts as not only a good current collector but also a catcher of dissolved sulfur.

The long-term cycling stability of S-DIB@CNT was also evaluated, and after cycling over 450 cycles at 1 C rate, the capacity remains at 647 mA h g^{-1}, corresponding to a capacity retention of 79% of its initial value at 1 C rate and a small capacity decay of 0.05% per cycle. The Coulombic efficiency is close to 100%, representing good performance for long-cycle Li—S batteries. Comparing the electrochemical performance of the S-DIB@CNT hybrid cathode with previously reported Li—S hybrid cathodes,[15,16,23–27] it can be clearly seen that the electrochemical performance of our material is significantly better, especially at high rates (Table S1, Supporting Information). Compared with the conventional physical confinement of polysulfides in porous carbon-based electrodes, the additional chemical confinement further restrains the polysulfide shuttle effect and increase the content of active sulfur in the electrode.

In summary, we have designed and prepared a hybrid cathode for Li—S batteries composed of CNTs partially filled with a sulfur copolymer. This structure benefits from both the physical confinement of polysulfide ions by CNT walls and the chemical confinement of sulfur by binding in the sulfur copolymer. The partially filled CNTs not only facilitate electron and ion transfer during charge–discharge, but also accommodates the sulfur volume expansion. The sulfur copolymer inside the CNT increases the Li^+ transfer rate by providing π electrons of the benzene ring and prevents the dissolution of lithium polysulfide ions by forming C—S bonds. With this strategy, this binder-free and metal current-collector-free electrode has a high specific capacity of 880 m Ah g^{-1} at 1 C after 100 cycles with a capacity retention of over 98%. Our dual-confinement strategy offers a new, efficient pathway for the fabrication of high-performance sulfur copolymer–carbon matrix electrodes for Li—S batteries.

Experimental Section

Preparation of S-DIB: The S-DIB was synthesized using a previously reported method.[21] In a typical synthesis procedure, sulfur powder (4.50 g, 17.6 mmol) was heated to 185 °C in a thermostat oil bath to obtain an orange molten phase. Then, a certain amount of DIB (0.5 g, 3.16 mmol) was dropped into the molten sulfur with a syringe to form a homogeneous mixture that was stirred at 185 °C for 10 min, and then allowed to cool to room temperature.

Preparation of S-DIB@CNT and S@CNT Hybrid Membranes: AAO (Whatman, Anodisc, Φ = 200–250 nm) membranes were used as templates for the preparation of CNT. Chemical vapor reduction and deposition were performed at 650 °C in a gas mixture (C_2H_2-20 sccm and N_2-200 sccm) for 4 h. The intermediate product of AAO/CNT membranes was obtained after the furnace was cooled to room temperature in pure N_2. Then the AAO/CNT membrane was dipped into molten S-DIB at 185 °C, so that the S-DIB filled the channels. Excess S-DIB covering the top and bottom surfaces of the membrane was removed by CS_2 washing. The alumina template was then etched with 5M NaOH solution for 12 h. The NaOH solution was rinsed away several times with DI water and the

S-DIB@CNT bundles were dispersed in ethanol. Finally, an S-DIB@CNT membrane was obtained using ultrasonication and vacuum filtration. The S@CNT membrane was prepared using a similar process.

Materials Characterization: The morphology and structure of the samples were characterized using a scanning electron microscope (SEM, FEI Nova Nano SEM 430, 15 kV) and a transmission electron microscope (TEM, Tecnai F20). TGA was performed with a NETZSCH STA 449 C thermos-balance in argon with a heating rate of 10 °C min^{-1} from room temperature to 600 °C. XPS analysis was performed using an ESCALAB 250 instrument with Al Kα radiation (15 kV, 150 W) under a pressure of 4×10^{-8} Pa. XRD was conducted with a D-MAX/2400 diffractometer (Cu Kα, $\lambda = 0.154056$ nm). Raman spectra were collected with a 532 nm laser under ambient conditions using a JY HR800 instrument with a laser spot size of 1 mm. ^{1}H and ^{13}C NMR spectra were recorded on a Bruker Avance 600 MHz spectrometer from samples in solution at room temperature. Chemical shifts (δ, ppm) were reported relative to tetramethylsilane (Me4Si).

Electrochemical Property Measurements: The electrode membrane was dried in an oven at 60 °C for 12 h, and cut into round disks with a diameter of 0.8 cm. The mass loading of the S-DIB@CNT and S@CNT electrodes was about 1.9–2.5 and 1.7–1.8 mg cm^{-2}, respectively. The electrolyte was prepared by dissolving lithium bistrifluoromethanesulphonylimide (99%, Acros Organics, 1 m) and lithium nitrate ($LiNO_3$, 99.9%, Alfa Asea, 0.2 m) in 1, 2-dimethoxyethane (99.5%, Alfa Asea), and 1,3-dioxolane (99.5%, Alfa Asea) (1:1 ratio, by volume). The ratio of sulfur to electrolyte was ≈34 g L^{-1} for the coin cell. 2025-type stainless steel coin cells were assembled inside an Ar-filled glove box using a Celgard 2400 membrane as separator and Li metal as anode. Charge–discharge measurements were carried out galvanostatically at various current densities over a voltage range of 1.7–2.8 V (vs Li/Li^+) using a battery testing system (LAND CT2001A). The current density set for the tests referred to the mass of sulfur in the cathode and varied from 0.1 to 2 C (1 C = 1675 m Ah g^{-1}).

Supporting Information

Supporting Information is available from the Wiley Online Library or from the author.

Acknowledgements

G.J.H and Z.H.S. contributed equally to this work. The authors acknowledge financial support from MOST (2016YFA0200100 and 2014CB932402) and the National Science Foundation of China (Grant Nos. 51521091, 51525206, 51372253, 51625203, 51272051, and U1401243), the Youth Innovation Promotion Association of the Chinese Academy of Sciences (No. 2015150), the Natural Science Foundation of Liaoning province (No. 2015021012), and "Strategic Priority Research Program" of the Chinese Academy of Sciences (XDA01020304, XDA09010104), the Key Research Program of the Chinese Academy of Sciences (Grant No. KGZD-EW-T06), and the CAS/SAFEA International Partnership Program for Creative Research Teams.

Received: July 20, 2016
Revised: October 14, 2016
Published online: December 30, 2016

[1] X. L. Ji, K. T. Lee, L. F. Nazar, *Nat. Mater.* **2009**, *8*, 500.
[2] J. Liang, Z. Sun, F. Li, H.-M. Cheng, *Energy Storage Mater.* **2016**, *2*, 76.
[3] J. Nelson, S. Misra, Y. Yang, A. Jackson, Y. Liu, H. Wang, H. Dai, J. C. Andrews, Y. Cui, M. F. Toney, *J. Am. Chem. Soc.* **2012**, *134*, 6337.
[4] Y. V. Mikhaylik, J. R. Akridge, *J. Electrochem. Soc.* **2004**, *151*, A1969.
[5] Z. Wei Seh, W. Li, J. J. Cha, G. Zheng, Y. Yang, M. T. McDowell, P. C. Hsu, Y. Cui, *Nat. Commun.* **2013**, *4*, 1331.
[6] a) C. Barchasz, J.-C. Leprêtre, F. Alloin, S. Patoux, *J. Power Sources* **2012**, *199*, 322; b) M. Yu, R. Li, M. Wu, G. Shi, *Energy Storage Mater.* **2015**, *1*, 51.
[7] a) G. He, X. Ji, L. Nazar, *Energy Environ. Sci.* **2011**, *4*, 2878; b) B. Zhang, X. Qin, G. R. Li, X. P. Gao, *Energy Environ. Sci.* **2010**, *3*, 1531; c) J. Schuster, G. He, B. Mandlmeier, T. Yim, K. T. Lee, T. Bein, L. F. Nazar, *Angew. Chem. Int. Ed.* **2012**, *51*, 3591; d) Z. Li, Y. Jiang, L. X. Yuan, Z. Q. Yi, C. Wu, Y. Liu, P. Strasser, Y. H. Huang, *ACS Nano* **2014**, *8*, 9295; e) S. R. Chen, Y. P. Zhai, G. L. Xu, Y. X. Jiang, D. Y. Zhao, J. T. Li, L. Huang, S. G. Sun, *Electrochim. Acta* **2011**, *56*, 9549; f) M. S. Kim, J. Jeong, W. I. Cho, W. Kim, *Nanotechnol.* **2016**, *27*, 125401; g) A. D. Roberts, X. Li, H. F. Zhang, *Carbon* **2015**, *95*, 268; h) G. Y. Xu, B. Ding, L. F. Shen, P. Nie, J. P. Han, X. G. Zhang, *J. Mater. Chem. A* **2013**, *1*, 4490; i) N. Jayaprakash, J. Shen, S. S. Moganty, A. Corona, L. A. Archer, *Angew. Chem. Int. Ed.* **2011**, *50*, 5904; j) K. Zhang, Q. Zhao, Z. L. Tao, J. Chen, *Nano Res.* **2013**, *6*, 38.
[8] a) J. Guo, Y. Xu, C. Wang, *Nano Lett.* **2011**, *11*, 4288; b) M. Sahoo, S. Ramaprabhu, *Electrochim. Acta* **2015**, *186*, 142; c) L. W. Ji, M. M. Rao, S. Aloni, L. Wang, E. J. Cairns, Y. G. Zhang, *Energy Environ. Sci.* **2011**, *4*, 5053; d) G. Y. Zheng, Y. Yang, J. J. Cha, S. S. Hong, Y. Cui, *Nano Lett.* **2011**, *11*, 4462; e) H. J. Peng, J. Q. Huang, M. Q. Zhao, Q. Zhang, X. B. Cheng, X. Y. Liu, W. Z. Qian, F. Wei, *Adv. Funct. Mater.* **2014**, *24*, 2772; f) S. Dorfler, M. Hagen, H. Althues, J. Tubke, S. Kaskel, M. J. Hoffmann, *Chem. Commun.* **2012**, *48*, 4097; g) H. J. Peng, W. T. Xu, L. Zhu, D. W. Wang, J. Q. Huang, X. B. Cheng, Z. Yuan, F. Wei, Q. Zhang, *Adv. Funct. Mater.* **2016**, *26*, 6351.
[9] Y. Liang, Z. Tao, J. Chen, *Adv. Energy Mater.* **2012**, *2*, 742.
[10] W. J. Chung, J. J. Griebel, E. T. Kim, H. Yoon, A. G. Simmonds, H. J. Ji, P. T. Dirlam, R. S. Glass, J. J. Wie, N. A. Nguyen, B. W. Guralnick, J. Park, A. Somogyi, P. Theato, M. E. Mackay, Y. E. Sung, K. Char, J. Pyun, *Nat. Chem.* **2013**, *5*, 518.
[11] Z. Sun, M. Xiao, S. Wang, D. Han, S. Song, G. Chen, Y. Meng, *J. Mater. Chem. A* **2014**, *2*, 9280.
[12] G. M. Zhou, D. W. Wang, F. Li, P. X. Hou, L. C. Yin, C. Liu, G. Q. Lu, I. R. Gentle, H. M. Cheng, *Energy Environ. Sci.* **2012**, *5*, 8901.
[13] F. Y. Jin, S. Xiao, L. J. Lu, Y. Wang, *Nano Lett.* **2016**, *16*, 440.
[14] H. J. Peng, J. Q. Huang, M. Q. Zhao, Q. Zhang, X. B. Cheng, X. Y. Liu, W. Z. Qian, F. Wei, *Adv. Funct. Mater.* **2014**, *24*, 2772.
[15] Z. Li, L. Yuan, Z. Yi, Y. Liu, Y. Xin, Z. Zhang, Y. Huang, *Nanoscale* **2014**, *6*, 1653.
[16] Z. Li, J. T. Zhang, X. W. Lou, *Angew. Chem. Int. Ed.* **2015**, *54*, 12886.
[17] H. Kim, J. Lee, H. Ahn, O. Kim, M. J. Park, *Nat. Commun.* **2015**, *6*, 7278.
[18] a) L. Ji, M. Rao, H. Zheng, L. Zhang, Y. Li, W. Duan, J. Guo, E. J. Cairns, Y. Zhang, *J. Am. Chem. Soc.* **2011**, *133*, 18522; b) H. Al Salem, G. Babu, C. V. Rao, L. M. Arava, *J. Am. Chem. Soc.* **2015**, *137*, 11542.
[19] C. Barchasz, F. Molton, C. Duboc, J. C. Lepretre, S. Patoux, F. Alloin, *Anal. Chem.* **2012**, *84*, 3973.
[20] M. V. Reddy, T. Yu, C. H. Sow, Z. X. Shen, C. T. Lim, G. V. S. Rao, B. V. R. Chowdari, *Adv. Funct. Mater.* **2007**, *17*, 2792.
[21] Y. Liang, Z. Tao, J. Chen, *Adv. Energy Mater.* **2012**, *2*, 742.
[22] B. Li, S. Li, J. Xu, S. Yang, *Energy Environ. Sci.* **2016**, *9*, 2025.
[23] H. B. Yao, G. Y. Zheng, W. Y. Li, M. T. McDowell, Z. W. Seh, N. A. Liu, Z. D. Lu, Y. Cui, *Nano Lett.* **2013**, *13*, 3385.
[24] M. Q. Zhao, X. F. Liu, Q. Zhang, G. L. Tian, J. Q. Huang, W. C. Zhu, F. Wei, *ACS Nano* **2012**, *6*, 10759.
[25] J. J. Chen, Q. Zhang, Y. N. Shi, L. L. Qin, Y. Cao, M. S. Zheng, Q. F. Dong, *Phys. Chem. Chem. Phys.* **2012**, *14*, 5376.
[26] D. L. Wang, Y. C. Yu, W. D. Zhou, H. Chen, F. J. DiSalvo, D. A. Muller, H. D. Abruna, *Phys. Chem. Chem. Phys.* **2013**, *15*, 9051.
[27] C. Wang, W. Wan, J. T. Chen, H. H. Zhou, X. X. Zhang, L. X. Yuan, Y. H. Huang, *J. Mater. Chem. A* **2013**, *1*, 1716.